A novel approach to estimate systematic and random error of terrain derived from UAVs: a case study from a post-mining site

***Rudolf Urban*[1], *Martin Štroner*[1], *Tomáš Křemen*[1], *Jaroslav Braun*[1] and *Michael Möser*[2]**

In recent years, there has been a major development in the field of Unmanned Aerial Vehicles (UAVs) as well as a significant increase in the use of aerial photogrammetry, which is an affordable alternative to using LiDAR. However, the nature of the data obtained from photogrammetry differs from LiDAR data. Photogrammetry using the Structure from Motion (SfM) method is however computationally complicated, and results can be affected by many influences. In this paper, data from two UAVs were compared. The first one is a commercial eBee system produced by SenseFly equipped with a Sony Cyber-shot DCS-WX220 camera. The other is a home assembled solution consisting of EasyStar II motorised glider and 3DR Pixhawk B autopilot equipped with Nikon Coolpix A camera. The area of spoil heap was measured by both systems in the leaf-off period. Both systems were set up identically for data acquisition (overlapping, resolution), which made a comparison of the output quality possible. The ground control points (GCPs) were placed in the study area and their position determined by GNSS (RTK method).

A traditional approach for point clouds accuracy validation is their comparison with data of greater accuracy. Unfortunately, the photogrammetry is often validated using GNSS points, the position of which is determined under different conditions than GCPs (different daytime, number, and visibility of satellites, etc.). The magnitude of photogrammetry errors is theoretically the same as that of GNSS. Therefore, in this study, we suggest a novel approach that can be used to compare the accuracy of UAV point clouds without the need for additional validation data (for example, GNSS survey). To exemplify this approach, we used data gathered by two UAV systems (eBee and Easy Star II). Particularly, we statistically estimated the accuracy of the UAV point clouds; used two approaches to estimate standard deviations (one of them using estimated dependencies between data); and investigated the influence of the vegetation cover.

To determine the systematic and random errors of the UAV systems data, three areas were selected, each with a typical example of vegetation on the spoil heap (forest, grass, bush). A comparison of the individual data in a grassy area suggests that the accuracy of the differences is about 0.03 m, which corresponds to the actual pixel size. Average shift (systematic error) ranged from 0.01 m to 0.08 m. In the forest terrain, the accuracy of data differences is about 0.04 m, which is slightly worse than in the grassy area. Bushy terrain data achieves precision values between a grassy area and a forest area.

Keywords: *digital terrain model (DTM), UAV, photogrammetry, spoil heap*

1. Introduction

Mining has a significant impact on the environment. From this point of view, the surface mines are particularly problematic with the original arrangement of the landscape completely disturbed and the fertile field taken away. Although the regeneration of these areas is usually incorporated into mining plans, the actual effect of these activities is still being investigated through scientific research.

Published studies typically use measurement data to model the current state of the landscape or to analyse terrain stability (for example, Close et al., 2016; Stephenne et al. 2014; Zalesky and Capova, 2017). Such data represent the basis, the frame, and their quality is conditional for the quality of the study results. Data are acquired in a variety of ways, including terrestrial geodetic techniques such as total station and/or GNSS measurements (for example, Hogarth et al., 2017; Zalesky et al., 2008). Such common methods are however more appropriate for targeting a limited number of individual points rather than to capture a larger natural area at the stage of standard bio-chaos. A great benefit of remote sensing over more traditional techniques lies in its ability to provide continuous information over a large area. However, references to the use of remotely sensed data for monitoring or restoration success assessment of post-mining sites are scarce (Ćmielewski, 2018; Cordell, 2017).

For such purposes, mass data acquisition technologies such as laser 3D scanning, photogrammetry, and satellite imagery are preferable to traditional techniques. Laser 3D scanning is especially suitable in its airborne variant known as Airborne Laser Scanning (ALS) or LiDAR (Light Detection And Ranging), where multiple reflections of a single signal/flight allow a comprehensive analysis of the condition of the vegetation and creation of a quality digital terrain model, used for example by (Koska, 2017) or by (Wężyk, 2015) for landscape monitoring.

Recently, extensive research into the use of UAVs carrying a digital camera has been performed. Data processing through photogrammetric methods based on Structure from Motion and/or Patch-based Multi-View

[1] *Rudolf Urban, Martin Štroner, Tomáš Křemen, Jaroslav Braun*, Czech Technical University in Prague, Faculty of Civil Engineering, Department of Special Geodesy, Thákurova 7, Prague 6, 166 29, Czech Republic, rudolf.urban@fsv.cvut.cz, martin.stroner@fsv.cvut.cz, tomas.kremen@fsv.cvut.cz, jaroslav.braun@fsv.cvut.cz

[2] *Michael Möser* , Technical University Dresden, Faculty of Environmental Sciences, Department of Geosciences, Geodetic institute. Hülsse-Bau, Westsight Helmholtzstraße 10, 01069 Dresden. Germany, michael.moeser@tu-dresden.de

Stereo is investigated, along with the use of a wide range of carriers and digital cameras from professional and costly to very inexpensive and simple. For example in (Pukanská, 2014) photogrammetry was used for mapping of a surface quarry and compared with the 3D scanning method, rock outcrops documentation by the UAV photogrammetry was studied by (Blišťan, 2016). Low-cost UAVs can also be successfully used for digital terrain modelling as shown by (Kršák, 2016). The digital terrain model built in this way can subsequently serve for various purposes such as for the monitoring of rock slides (Fraštia, 2014), a case of the monitoring of the Super-Sauze landslide is described by (Niethammer, 2012). Degradation of the coastal areas is another field of research where the UAVs can be successfully used according to (Goncalves, 2015). Roads detection is another of UAV applications (Zhou, 2015). Monitoring of the dynamic natural processes with a focus on reproducibility of the Earth topography is described in (Claypuyt, 2016). A similar topic focusing on a river channel evolution is investigated in (Flener, 2013) combining mobile laser scanning and low-altitude unmanned aerial vehicle photography for creating both a bathymetric model and DTM of a meandering Sub-arctic River. The disadvantage is the need to take pictures or perform the measurement during the leaf-off period to be able to obtain a terrain model as documented in (Hogson, 2005)

Numerous UAV platforms equipped with various cameras are increasingly available on the market, differing in their suitability for mapping of mining areas (Thoeni et al., 2014; Boon, Drijfhout, and Tesfamichael, 2017; Torresan et al., 2017). Surveyors then often face a question which UAV platform to buy. The ever-increasing use of UAVs for mining industry makes the knowledge of the precision of resulting point clouds very important. Experimental flights over typical areas with various UAVs are often performed before committing to the purchase.

A traditional approach for point clouds accuracy validation is their comparison with data of greater accuracy. Unfortunately, the photogrammetry is often validated using GNSS points, the position of which is determined under different conditions than GCPs (different daytime, number, and visibility of satellites, etc.). The magnitude of photogrammetry errors is theoretically the same as that of GNSS. The point cloud accuracy can be greatly affected by the accuracy of the GCP for the GNSS. Due to the size of the image overlays and flight height (actual pixel size), the internal accuracy of the photogrammetric model may be higher than the accuracy of the GCP determination. Another disadvantage when comparing a point cloud with the GNSS point is that the collection of validation data is often limited to hard surfaces and easily accessible places. Another option is to compare point cloud with airborne laser scanning data; those are however also affected by a GNSS error. Ideal data for comparison would be data identifying both GCPs and validation points in random cloud places, determined with significantly higher accuracy than that expected of the model itself. Such validation data can be obtained using a total station method that has a significantly higher accuracy than GNSS but is quite a time-consuming and thus economically demanding.

Therefore, in this study, we suggest a novel approach that can be used to compare the accuracy of UAV point clouds without the need for additional validation data (for example, GNSS survey). To exemplify this approach, we used data gathered by two UAV systems – a commercially available eBee and home–assembled Easy Star II fixed wing system. Particularly, we (1) statistically estimated the accuracy of the UAV point clouds; (2) used two approaches to estimate standard deviations; and (3) investigated the influence of the vegetation cover

2. Materials and Methods

2.1 Hornojiřetínská spoil heap

Spoil heap (Fig. 1) is located in north-west Bohemia, Czech Republic, in the Most mining district (50°34’N, 13°34’E). The study area of 68 ha is located in the southern part of Hornojiřetínská spoil heap, which has not been technically reclaimed. The terrain morphology has, as a result, remained rugged with a typical undulated terrain formed by heaping (for example, Doležalová et al., 2012). It has been observed that rough terrain and dense vegetation negatively affect the accuracy of point clouds (for example, Meng et al., 2010). Therefore, such a challenging environment provides an ideal location for exploring the quality of point clouds and DTMs.

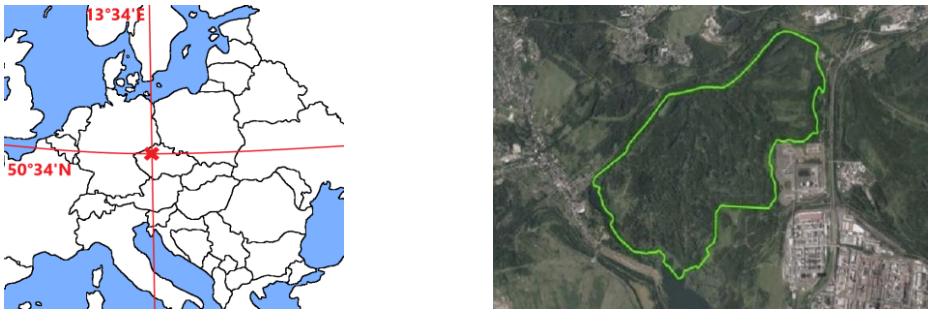

Fig. 1. Location of the Hornojiřetínská spoil heap.

Before the UAV flights, twenty ground control points (GCPs) were established within and in the vicinity of the study area (Fig. 2, yellow dots with blue flags). GCPs were made of white wooden boards (dimensions 0.40m by 0.40m) with a black circle of 0.15m diameter in the centre. The expected pixel dimension of the circle in the image at the intended resolution and flight height was approximately 5 x 5 pixels. GCP coordinates were surveyed using a Trimble GeoXR 6000 handheld GNSS receiver with Zephyr 2 external antenna mounted on a pole, by the dual-frequency real-time kinematic (RTK) method with a 15 seconds observation time, with a connection to the CZEPOS permanent GNSS network. All GCPs were transformed to the Datum of Uniform Trigonometric Cadastral Network (S-JTSK; EPSG: 5514) and Baltic Vertical Datum - after adjustment (Bpv; EPSG: 5705). Relative precision of GCPs can be estimated at 0.02 m (for example, Štroner et al., 2013).

Fig. 2. Location of the study areas (red rectangles - forested area (central part), bushy area (upper left corner) and grassy area (lower left corner); GCPs marked as yellow dots with blue flags.

The whole area of the spoil heap consists of distinctly different zones with regard to surface cover, ranging from dense forest through low bushes to surface solely covered by grass. Three zones with those three types of vegetation were selected as study areas (red rectangles at Fig. 2).

2.2 UAV systems

Two UAV systems were used for image collection. A commercial system EBee (Fig. 3) produced by the SenseFly company is a fixed-wing aircraft with removable wings and a push propeller. It allows an automatic flight with a flight time of up to 40 minutes. It is a commercially available mapping and monitoring system for data acquisition, equipped with a complete control unit. For the experiment, the aircraft was equipped with a SenseFly provided Sony Cyber-shot DSC-WX220 camera (pixel size 1.25 μm) with a resolution of 18.2 MPix and a focal length of 4.45 to 44.5mm (was set to 4.45 mm during acquisition, a 35mm equivalent 25mm).

Home-assembled drone EasyStar II is a commercially available motor glider (Fig. 3), which can be combined with a commercially available 3DR Pixhawk autopilot. This autopilot can convert any type of model into an autonomous system. The system also features a Nikon Coolpix A (pixel size 1.19 μm) camera with a 16.2-megapixel resolution and a fixed focal length of 18.5mm (35mm equivalent 28 mm).

Fig. 3. Ebee (left) and Easystar (right).

2.4 UAV surveys

UAV images were collected during March 2017. One flight with Easystar and two flights with eBee were performed to assess the effect of the image quantity on the accuracy and density of a point cloud. The eBee flights were mutually perpendicular and differed in flight trajectories (Fig. 4). From now on, we refer to these flights as Easystar, eBee[1,] and eBee[2]. For both systems, a forward overlap of 85 %, sidelap of 65 % and a ground

sampling distance of about 30 mm per pixel was set. The height and speed of the UAV flight, as well as the shutter speed (1/250 – 1/ 640 for Ebee and 1/1250 for Easystar), were set in both systems by the control program. For both systems, the flight height was about 100 m above the ground level. During the Ebee flights, the weather was sunny with a temperature of 19 °C, and during the Easystar flight, it was partly sunny with 8 °C. For the eBee system, two complete mutually perpendicular flights were performed. The first flight yielded 1004 images (marked as eBee 1, Fig. 4 left) and the second one 903 images (marked as eBee 2, Fig 4 middle). Only one flight (940 images, Fig. 4 right) was performed with the Easystar II glider.

Fig. 4. Flight line trajectories (from left eBee[1](left), eBee[2](middle) and Easystar (right).

2.5 Image processing and 3D point cloud generation

To generate 3D point clouds, acquired images were processed in the Agisoft's PhotoScan Professional software, version 1.2.6. Processing was done separately for each individual flight (Easystar, eBee[1], eBee[2]) as well as for the combination of the two eBee flights (eBee[12]) to test the improvement in the terrain representation. The process consisted of alignment, iteratively refining external and internal camera orientations and camera locations through a least squares method, thus generating a sparse point cloud of tie points, followed by an application of a dense multi-view 3D surface reconstruction algorithm. The images, along with a text file containing camera positions estimated by the onboard GNSS during the flight, were loaded into PhotoScan software. The alignment was subsequently completed using the accuracy parameter set to "high" and pair pre-selection to "disabled". Accuracy set to "high" ensured that the original resolution of images was used while the "disabled" pair pre-selection ensured the most accurate image matching in all possible combinations. The limit for key points (indicating the maximum number of points sampled within each image) was set to 20,000 and for tie points (points used for image matching and relative orientation) to 5,000. The GCPs were loaded and identified in the images, their a priori accuracy was set to 0.02 m. Six ground control points were completely removed from the evaluation due to their physical displacement or complete destruction by animals. This devaluation was caused by a time gap between the measurement of the ground control points and the flights, which was in turn caused by the necessity to wait for the appropriate weather conditions (no snow cover, low wind speed, etc.). Bundle adjustments were computed in the S-JTSK and Bpv datum. Dense point clouds were built with a high reconstruction quality and mild depth filtering (set in software Agisoft for optimal results in our study area). To determine the accuracy of the photogrammetric model, the total coordinate error (TCE) was calculated for each point cloud as follows:

$$\Delta_{pi} = \sqrt{\Delta_{xi}^2 + \Delta_{yi}^2 + \Delta_{zi}^2}, \tag{1}$$

where Δ_{xi} , Δ_{yi} , Δ_{zi} are coordinate differences of ground control points.

$$TCE = \sqrt{\frac{\Delta_{p1}^2 + \Delta_{p2}^2 + \cdots + \Delta_{pn}^2}{n}}. \tag{2}$$

The point clouds were exported to the LAS format, and points representing ground surface were identified using LAS Ground tool in the ArcGIS software. We calculated point clouds density and height differences between point clouds in Cloud Compare 2.9.1. The entire workflow is illustrated in Fig. 5.

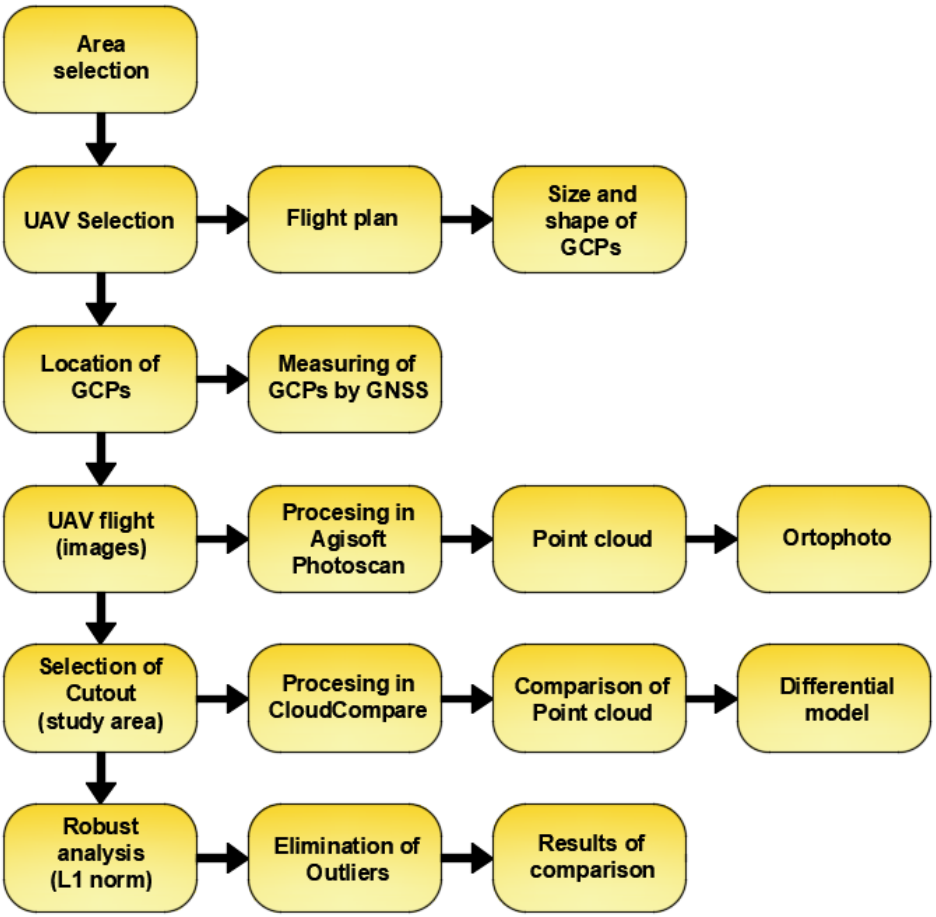

Fig. 5. The whole procedure diagram.

The total coordinate error of the point clouds in Agisoft Photoscan from eBee achieved worse results than Easystar, which was most likely caused by the lower quality of images. These results were published in (Moudrý, 2018) and are given in Tab. 1 for a general description of each flight and its processing.

Tab. 1. Precision overview of flights.

Flight	Total coordinate error [m]
Easystar	0.041
eBee[1]	0.081
eBee[2]	0.053
eBee[12]	0.050

Residual errors from the Coolpix A camera (Easystar) after calibration in a maximum of 0.2 pixels were very small, which is most likely due to the construction and superior quality of the lens. The DSC-WX220 camera (eBee) achieved a residual error after calibration in a maximum of 0.7 pixels.

2.6 Outliers filtering

Due to the presumed presence of outliers, we used a robust method (L1 norm). This method (Koch, 1999), as a function of the probability distribution, directly uses Laplace distribution that is more suitable for data with outlying values than a normal distribution. For nonhomogeneous measurements (measurements with the different standard deviation) a robust weight change is given by the function,

$$w_i = 1 / |v_i|. \quad (3)$$

Where w_i represents weights and v_i residuals. The calculation is done iteratively, residuals acquired from one calculation are used to calculate robust weights' changes in the next calculation. The outliers are determined by residuals exceeding the limit value (2.5 times the standard deviation calculated from residuals before the robust method use). After detection and exclusion of the first set of outliers, a new value of mean and standard

deviation is determined, followed by a new robust analysis of outliers. The algorithm of outliers' filtration is shown in Fig. 6.

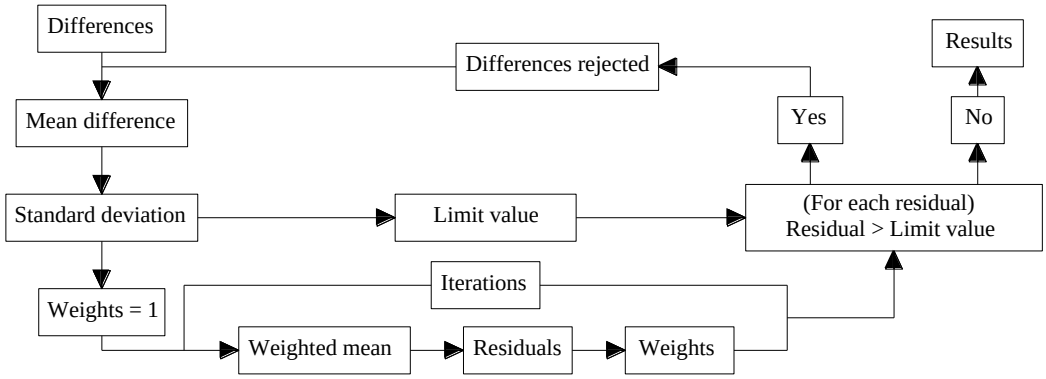

Fig. 6. Algorithm of outliers' filtration.

Ten iterations were typically used, and the number of outliers did not exceed 5 % of the dataset. From the point clouds representing the bare ground, the following vertical differences were calculated: EasyStar - eBee1, Easystar – eBee2, Easystar – eBee12, eBee1 – eBee2, eBee1 – eBee12 and eBee2 – eBee12. These differences were used for calculating a mean difference (which is the difference between systematic errors) and the standard deviation of the differences (describing the random errors). The RMSE of the differences consists of systematic error and random error while the standard deviation contains only the random error component.

$$\text{Mean difference} = \frac{\sum_{i=1}^{N}(x_i - x_{REF})}{N} \tag{4}$$

$$\text{RMSE} = \sqrt{\frac{\sum_{i=1}^{N}(x_i - x_{REF})^2}{N}} \tag{5}$$

$$\text{Standard deviation} = \sqrt{\frac{\sum_{i=1}^{N}(x_i - \bar{x})^2}{N-1}} \tag{6}$$

where x_i is the elevation derived from the first point cloud, x_{REF} is the corresponding elevation in the second point cloud, and N is the number of differences. Differences were derived using 2.5D Delaunay triangulation from ten nearest points in the software Cloud Compare 2.9.1.

2.7 Evaluation of correlated data

In principle, it is not possible to calculate the absolute precision and accuracy characteristics just from the differences. In the presented experiment, the differences and their standard deviations were calculated in all six possible combinations (EasyStar - eBee1, Easystar – eBee2, Easystar – eBee12, eBee1 – eBee2, eBee1 – eBee12 and eBee2 – eBee12).

The fact that some of the differences were calculated from partly identical data (i.e., eBee12 is a combination of images also used for eBee 1 and eBee 2 point cloud, respectively), and are therefore self-correlated had to be taken into account. An equation describing the relation of the single standard deviations of individual point clouds (data "a" and "b") and the standard deviation of their difference is:

$$\sigma_a^2 + \sigma_b^2 = \sigma_{\Delta ab}^2 \tag{7}$$

Where σ_a^2 is stthe andard deviation of the first point cloud, σ_b^2 of the second point cloud and $\sigma_{\Delta ab}^2$ is a standard deviation of their difference. In our case, only the standard deviation of the difference was known. However, due to the existence of four point clouds in total, there are six of these equations with four unknowns to solve (standard deviations of each point cloud). Due to the possible correlation of the data (differences of point clouds) to the calculation, a variance - covariance matrix must be added. Formulas for the calculation of surface coordinate points from th eimagery is very complicated and the size of the correlation can therefore be only estimated.

Authors have chosen to use the multiple generation of three random files E1, E2, E3 (each containing 1000 randomly generated numbers). File E4 was created as a sum of E1 and E2 (like Ebee12 = Ebee1 + Ebee2), after which the differences L1 – L6 and standard deviations of differences were calculated.

$$\begin{aligned} &L1 = E1 - E2; \ldots s_{\Delta 12} \\ &L2 = E1 - E3; \ldots s_{\Delta 13} \\ &L3 = E1 - E4; \ldots s_{\Delta 14} \\ &L4 = E2 - E3; \ldots s_{\Delta 23} \\ &L5 = E2 - E4; \ldots s_{\Delta 24} \\ &L6 = E3 - E4; \ldots s_{\Delta 34} \end{aligned} \tag{8}$$

The data are only subtracted, each difference L1 … L6 is characterised by the standard deviation s, which is the result of the real data subtraction. The dependence of the data thus determined can be characterized by a correlation coefficient, which can easily be converted to covariance. If the standard deviation of the individual variables is equal to 1, the correlation coefficient is directly the covariance.

The correlation coefficient ρ can be easily calculated using a definition formula:

$$\rho = \frac{s_{xy}}{s_x \cdot s_y}, \tag{9}$$

where

$$s_x = \sqrt{\frac{v'^2_x}{n-1}}, \; s_y = \sqrt{\frac{v'^2_y}{n-1}}, \; s_{xy} = \frac{v'_x \cdot v'_y}{n-1}. \tag{10}$$

The v_x and v_y are corrections from the mean within individual files L1 … L6 and n is the number of differences for each dataset L1 … L6. Due to the relatively small dataset and pseudo-randomness of computer-generated random numbers (common rand() function), generation and computation were performed 1000x, and the mean was used as a result. The resulting correlation matrix **M** shows considerable dependencies:

$$\boldsymbol{M} = \begin{pmatrix} 1 & 0.50 & 0.51 & -0.50 & 0.50 & 0.51 \\ 0.50 & 1 & 0.51 & 0.50 & 0.50 & 0.49 \\ 0.51 & 0.51 & 1 & 0 & 1 & 1 \\ -0.50 & 0.50 & 0 & 1 & 0.01 & -0.01 \\ 0.5 & 0.50 & 1 & 0.01 & 1 & 1 \\ 0.51 & 0.49 & 1 & -0.01 & 1 & 1 \end{pmatrix} \tag{11}$$

This correlation and covariance matrix were used for the calculation of the solution of the system of equations for the determination of the individual standard deviations. A plan matrix **A**:

$$\boldsymbol{A} = \begin{pmatrix} 1 & 1 & 0 & 0 \\ 1 & 0 & 1 & 0 \\ 1 & 0 & 0 & 1 \\ 0 & 1 & 1 & 0 \\ 0 & 1 & 0 & 1 \\ 0 & 0 & 1 & 1 \end{pmatrix} \tag{12}$$

The measurement vector **l** is given by the standard deviations of the differences in the square, and thus:

$$\boldsymbol{l} = \begin{pmatrix} s^2_{\Delta Easystar,eBee1} \\ s^2_{\Delta Easystar,eBee2} \\ s^2_{\Delta Easystar,eBee12} \\ s^2_{\Delta eBee1,eBee2} \\ s^2_{\Delta eBee1,eBee12} \\ s^2_{\Delta eBee2,eBee12} \end{pmatrix} \tag{13}$$

The weight matrix $\boldsymbol{P}$ is acquired according to the formula:

$$P = M^{-1} \tag{14}$$

The system of equations is then solved by the least squares method easily, as it is in a linear form (unknown standard deviations are also solved in square):

$$\begin{pmatrix} s^2_{Easystar} \\ s^2_{eBee1} \\ s^2_{eBee2} \\ s^2_{eBee12} \end{pmatrix} = (\mathbf{A}^{\mathrm{T}} \cdot \mathbf{P} \cdot \mathbf{A})^{-1} \cdot \mathbf{A}^{\mathrm{T}} \cdot \mathbf{P} \cdot \mathbf{l}\,. \tag{15}$$

To show the advantage of our method, we also tested the approach without the use of a weight matrix (no correlation calculation).

3. Results and discussion

3.1 Comparison of point clouds

The density of point clouds for the acquired data sets varied significantly (Tab. 2). The densest point cloud was achieved with Easystar in all areas.

Tab. 2. Mean point density of study areas (points per m^2).

Flight	Forest	Grass	Bushy
Easystar	313	275	309
eBee^1	249	250	266
eBee^2	185	181	196
eBee^{12}	217	223	239

Tab. 3 shows a comparison of data in a height component for a grassy area. The mean difference values (systematic shift) are about 0.05 m higher for Easystar data in comparison to all eBee data. Ebee data shows similar parameters with very small systematic shift, which corresponds to the size of one pixel in reality. The values of the standard deviations for all data combinations show similar values up to 0.03 m.

Therefore, the quality of the camera does not have a significant effect on the relative accuracy of the model but directly affects the systematic shift of the whole model (determination of the points) and the number of correctly evaluated points (Tab. 2).

It is also interesting to note that on the grassy surface, a very small number of outlying points were detected in comparison to other surfaces, although the surface is very compact, has a uniform colour and the correlation of individual pixels in the picture may not be unambiguous.

Tab. 3. Grass area.

Data difference	Mean difference [m]	RMSE [m]	Std. deviation [m]	No. of differences	No. of outliers
Easystar - eBee^1	0.077	0.082	0.029	496757	2201 (0.44 %)
Easystar – eBee^2	0.046	0.054	0.029	365160	1225 (0.34 %)
Easystar – eBee^{12}	0.057	0.063	0.026	448186	1428 (0.32 %)
eBee^1 – eBee^2	0.029	0.041	0.029	365223	484 (0.13 %)
eBee^{12} – eBee^1	0.018	0.031	0.024	496508	1079 (0.22 %)
eBee^{12} – eBee^2	0.010	0.018	0.015	365044	1812 (0.50 %)

Fig. 7 shows a significant local distortion of the difference model between EasyStar and eBee 1 data (in the middle). On the right side, a comparison of the eBee 12 and eBee 2 is shown, which displays very small differences without significant deformation.

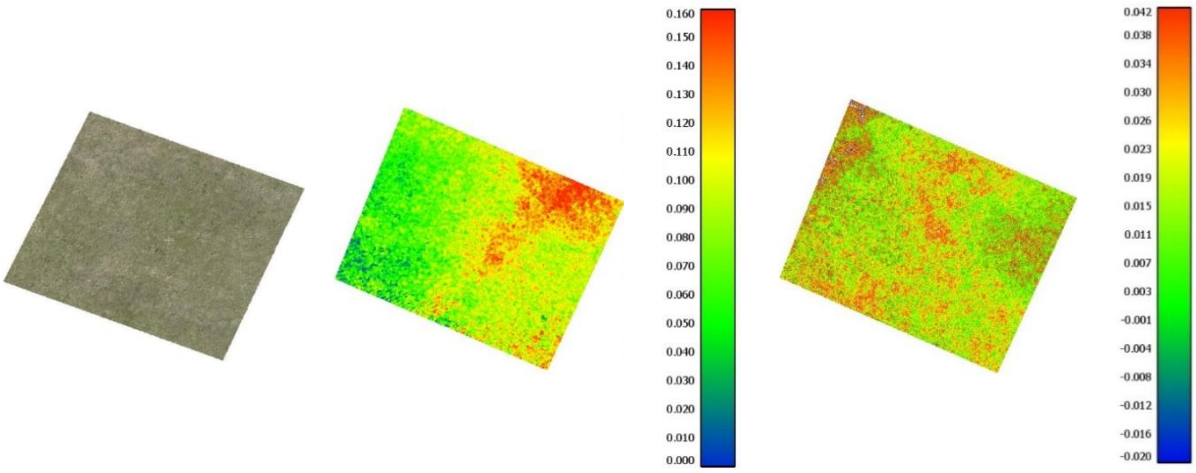

Fig. 7. Height differences of grassy area (Ortophotomosaic - left, Easystar vs. eBee1 – middle, eBee12 vs. eBee2 – right).

Tab. 4 shows a data comparison for a forested area. Values of mean differences point to a large systematic shift between both eBee 1 and 2 data, which reaches about 0.1 m. The values of the standard deviations of all data differences show values of about 0.04 m, which is slightly worse than in the grassy area. The number of outlying values is much higher, probably due to considerable filtration and generally worse evaluation quality due to the vegetation cover of the area. Despite these negative aspects, it is surprising that the coverage of the points (shown in Table 2) is not significantly worse than for the remaining surfaces.

Tab. 4. Forested area.

Data difference	**Mean difference** [m]	**RMSE** [m]	**Std. deviation** [m]	**No. of differences**	**No. of outliers**
Easystar - eBee^{1}	0.043	0.062	0.044	541920	9321 (1.72 %)
Easystar – eBee^{2}	0.062	0.074	0.039	413272	4942 (1.20 %)
Easystar – eBee^{12}	0.022	0.044	0.039	470317	7347 (1.56 %)
eBee^{1} – eBee^{2}	0.103	0.116	0.055	415704	6380 (1.53 %)
eBee^{12} – eBee^{1}	0.065	0.078	0.043	545399	12449 (2.28 %)
eBee^{12} – eBee^{2}	0.034	0.052	0.039	416149	9462 (2.27 %)

Fig. 8 shows the comparison of Easystar and eBee 12 data (middle), characterised by very small differences and clearly visible holes after ground filtration (tree removal). Fig. 8 shows on the right the differences between eBee 1 and eBee 2 data; especially in places where trees obscured the ground, large systematic shifts up to 0.25 m were detected, probably due to the different directions of the flight.

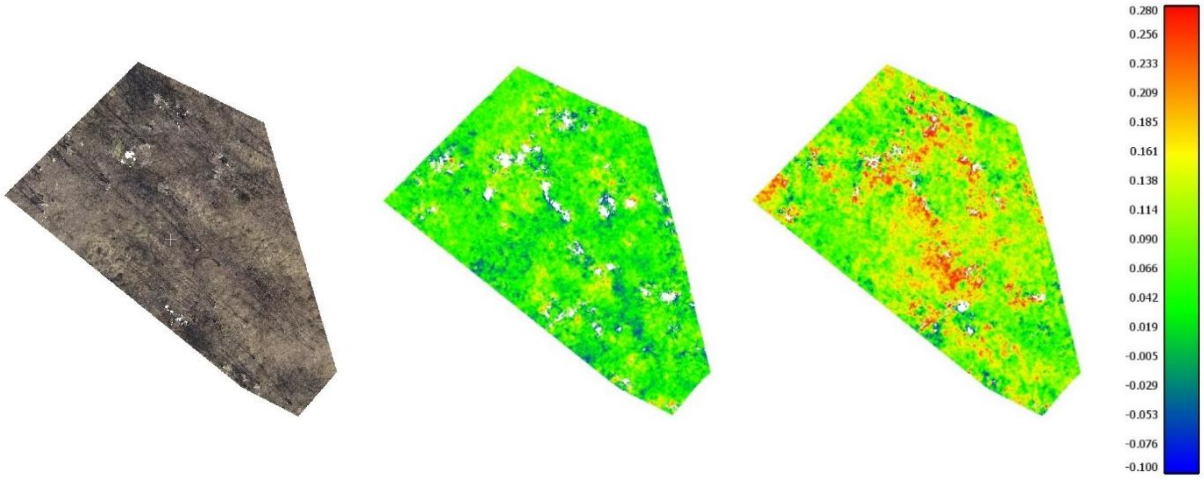

Fig. 8. Height differences of forested area (Ortophotomosaic – left, Easystar vs. eBee12 – middle, eBee1 vs. eBee2 – right).

Tab. 5 shows a comparison of data for the bushy area. The mean difference values are the smallest of all tested areas, which may be due to the proximity of three ground control points. Values of standard deviations are between the wooded area and the grassy area as expected. The number of outliers is similar to the forested area.

Tab. 5. Bushy area.

Data difference	**Mean difference** [m]	**RMSE** [m]	**Std. deviation** [m]	**No. of differences**	**No. of outliers**
Easystar - eBee^{1}	0.054	0.070	0.043	461261	9582 (2.08 %)
Easystar – eBee^{2}	0.013	0.037	0.034	339136	6419 (1.89 %)
Easystar – eBee^{12}	0.037	0.052	0.036	411331	6613 (1.61 %)
eBee^{1} – eBee^{2}	0.041	0.052	0.031	340180	5026 (1.48 %)
eBee^{12} – eBee^{1}	0.019	0.033	0.027	463081	8635 (1.86 %)
eBee^{12} – eBee^{2}	0.021	0.032	0.023	340566	4059 (1.19 %)

Fig. 9 shows in the middle the height differences of Easystar and eBee 1 data, where a greater height differences were found (red, yellow colour). Fig. 9 on the left, the height differences between Easystar and eBee 2 data are depicted, with fewer significant deformations or holes. So eBee 1 seems to be the worst in bushy and forest terrain.

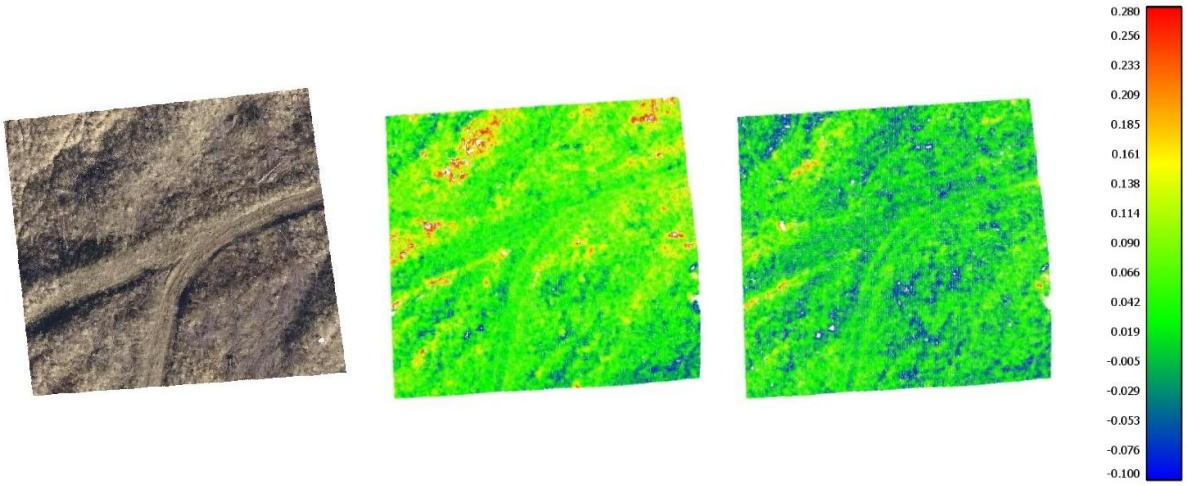

Fig. 9. Height differences of the bushy area (Ortophotomosaic, Easystar vs. eBee1 – left, Easystar vs. eBee2 – right).

3.2 Evaluation of data correlation

Results of the correlated data calculation, the estimates of the errors of each dataset are shown in Tab. 6, both variants (with and without the use of the weights and covariances) are presented.

Tab. 6. Estimation of the standard deviations from the correlated data.

Flights	**Forested area** [m]		**Grassy area** [m]		**Bushy area** [m]	
	No correlation used	Correlation	No correlation used	Correlation	No correlation used	Correlation
Easystar	0.024	0.038	0.023	0.023	0.033	0.037
eBee 1	0.039	0.041	0.022	0.021	0.026	0.029
eBee 2	0.034	0.037	0.017	0.009	0.015	0.025
eBee 12	0.023	0.031	0.008	0.010	0.014	0.018

The standard deviations determined by the adjustment with the use of the covariances are greater than the standard deviations determined without correlation usage, which is due to "false" internal compliance of (at least) a part of the data – in this case, a substantial part of the data. In addition, besides the increase of the values, their order in terms of accuracy changes, which is again caused by the dependencies (covariances). Covariances (or correlation coefficients) are estimates of the size dependencies, but their exact calculations are not possible in this case; on the other hand, but without the correction on covariances, the values can be considered to be more accurate than they really are since the data and its differences are highly dependent on each other. The values of standard deviations determined this way are also closer to realistically achievable values.

4. Summary

Here, we presented a comparison of data acquired through two UAV systems on a spoil heap in areas with various vegetation densities in the leaf-off stage. The first system was eBee (SenseFly), and the other was a home-assembled EasyStar II motor glider with 3DR Pixhawk autopilot. Images were processed in the same way using the same ground control points for both platforms to make the resulting data comparable in terms of random and systematic errors. These errors are, among other things, dependent on the used camera and its lens

distortion and internal imaging settings. For example, eBee keeps changing both shutter speed and ISO settings for the image capture while the Easystar system allowed the change of the aperture setting only.

To determine the systematic and random errors of the UAV-acquired data, three areas with typical examples of vegetation on the spoil heap were selected (forest, grass, bush). The density of the datasets was also determined for each area to compare the SfM efficiency of individual systems in different types of terrain. From the comparison of the densities of points in individual regions, it is evident that SfM yielded the best results in most cases in the bushy terrain. Interestingly, the density is the same or worse in the grassy area than in the forest area, where obscuring of the ground by the tree can be assumed. This phenomenon is probably caused by a worse matching of the relatively monochromatic grassy surface.

A comparison of the individual data on a grassy area suggests that the accuracy of the differences is about 0.03 m, which corresponds to the actual pixel size at the used flight height. However, individual data may show local deformations due to the worse quality of matching of points on the monochromatic surface. Average shift (systematic error) ranged from 0.01 m to 0.08 m. In the forested terrain, the accuracy of data differences is about 0.04 m, which is slightly worse than the in the grassy area. However, a large number of outlying values is present in the data, and the average value shows the greatest deviation of up to 0.12 m in the case of the two datasets acquired by the same system (eBee). Bushy terrain data achieves precision values between a grassy area and a forested area.

The evaluation of the data using simulated correlation values shows another side of the experiment. It indicates that such calculations can be treacherous if not calculated and interpreted well. Although the results achieved with and without the use of the simulated correlation data were relatively similar, these results differ in absolute values. When using the correlation data, standard deviations are higher, taking in account the inner dependence of individual used data. These standard deviations can be considered to be an estimate of the standard deviation describing the absolute precision of the data. It should be emphasised that this is only a statistical estimate, not the real values. Actual values of standard deviations cannot be determined in this way, a component of the mutual systematic error for both compared data will always be missing.

Acknowledgment*:This work was supported by the Grant Agency of the Czech Technical University in Prague, grant No. SGS18/067/OHK1/1T/11.*

References

Blišťan, P., Kovanič, Ľ, Zelizňaková, V., Palková, J. (2016) Using UAV photogrammetry to document rock outcrops. Acta Montanistica Slovaca, Volume 21, number 2, pp. 154-161, ISSN 1335-1788.

Boon, M. A., Drijfhout, A. P., Tesfamichael, S. (2017). Comparison of a Fixed-Wing and Multi-Rotor Uav for Environmental Mapping Applications: a Case Study. *The International Archives of Photogrammetry, Remote Sensing and Spatial Information Sciences, 42, 47.*

Clapuyt, F., Vanacker, V., Van Oost, K. (2016) Reproducibility of UAV-based earth topography reconstructions based on Structure-from-Motion algorithms. GEOMORPHOLOGY Volume: 260 Special Issue: SI Pages: 4-15.

Close, O., Stéphenne, N., Frippiat, C. (2016) Impact of DEM Processing on the Geotechnical Instability Analysis of Waste Heaps in Wallonia.GEOProcessing 2016: The Eighth International Conference on Advanced Geographic Information Systems, Applications, and Services. ISBN: 978-1-61208-469-5.

Cordell, S., Questad, E. J., Asner, G. P., Kinney, K. M., Thaxton, J. M., Uowolo, A. ... Chynoweth, M. W. (2017). Remote sensing for restoration planning: how the big picture can inform stakeholders. *Restoration Ecology, 25, S147-S154. ISSN: 1526-100X.*

Ćmielewski, B., Dabek, P. B., Patrzałek, C., Wilczynska, I. (2018). Potential of Using Unmanned Aircraft Systems for Landslide Monitoring: the Case of Janowiec Landslide in Poland. *Journal of Environmental Science and Management, 21(1). ISSN 0119-1144.*

Doležalová, J., Vojar, J., Smolová, D., Solský, M., Kopecký, O. Technical reclamation and spontaneous succession produce different water habitats: a case study from Czech post-mining sites. *Ecological engineering, 43: 5-12. doi:10.1016/j.ecoleng.2011.11.017*

Flener, C., Vaaja, M., Jaakkola, A. et al. (2013) Seamless Mapping of River Channels at High Resolution Using Mobile LiDAR and UAV-Photography. *REMOTE SENSING Volume: 5 Issue: 12 Pages: 6382-6407.*

Fraštia M., Marčiš M., Kopecký M., Liščák P., Žilka A. (2014) Complex geodetic and photogrammet-ric monitoring of the Kraľovany rock slide. In *Journal of Sustainable Mining. Vol. 13, no. 4, s. 12-16. ISSN 2300-1364.*

Goncalves, J. A., Henriques, R. (2015) UAV photogrammetry for topographic monitoring of coastal areas. *ISPRS JOURNAL OF PHOTOGRAMMETRY AND REMOTE SENSING Volume: 104 Pages: 101-111*

Hodgson, M. E., Jensen, J., Raber, G., Tullis, J., Davis, B., Thompson, G., Schuckman, K. An Evaluation of Lidar-derived Elevation and Terrain Slope in Leaf-off Conditions. *Photogrammetric Engineering & Remote Sensing, 71(7), 817–823.* http://doi.org/10.14358/PERS.71.7.817

Hogarth, J., Hawley, M., Beale, G. (2017) Instrumentation and monitoring. In Hawley, M., & Cunning, J. (Eds.), Guidelines for Mine Waste Dump and Stockpile Design. *CSIRO PUBLISHING*.

Koch, K. R. (1999) Parameter Estimation and Hypothesis Testing in Linear Models. *Springer Verlag, Berlin Heidelberg New York, ISBN 3-5406525-74.*

Koska, B., Jirka, V., Urban, R., Křemen, T., Hesslerová, P., Jon, J., Pospíšil, J., Fogl, M. (2017) Suitability, characteristics, and comparison of an airship UAV with lidar for middle size area mapping, *International Journal of Remote Sensing. 38(8-10), 2973-2990. ISSN 0143-1161*.

Kršák B., Blišťan, P., Pauliková, A., Puškárová, P., Kovanič, Ľ. ml., Palková, J., Zelizňaková, V. (2016) Use of low-cost UAV photogrammetry to analyze the accuracy of a digital elevation model in a case study. *Measurement. Vol. 91, p. 276–287. ISSN 0263-2241*.

Meng, X., Currit, N., Zhao, K. (2010). Ground filtering algorithms for airborne LiDAR data: A review of critical issues. *Remote Sensing, 2(3), 833–860*. http://doi.org/10.3390/rs2030833

Moudrý, V., Urban, R., Štroner, M., Komárek, J., Brouček, J., Prošek, J. (2018) Comparison of a commercial and home-assembled fixed-wing UAV for terrain mapping of a post-mining site under leaf-off conditions. International *Journal of Remote Sensing. 1 – 18.*

Niethammer, U., James, M. R., Rothmund, S. et al. (2012) UAV-based remote sensing of the Super-Sauze landslide: Evaluation and results. *ENGINEERING GEOLOGY Volume: 128 Special Issue: SI Pages: 2-11*

Pukanská, K., Bartoš, K., Sabová, J. (2014) Comparison of Survey Results of the Surface Quarry Spišské Tomášovce by the Use of Photogrammetry and Terrestrial Laser Scanning. In: *Inżynieria Mineralna. Vol. 33, no. 1, p. 47-54. ISSN 1640-4920.*

Stephenne, N., Frippiat, C., Veschkens, M., Salmon, M., Pacyna, D. (2014). Use of a LiDAR high resolution digital elevation model for risk stability analysis. *EARSeL eProceedings, 13(S1), 24-29.*

Štroner, M., Urban, R., Královič, J. (2013) Testing of the relative precision in local network with use of the Trimble Geo XR GNSS receivers. *Reports on Geodesy [online]. 94: 27-36*. https://doi.org/10.2478/rgg-2013-0004

Thoeni, K., Giacomini, A., Murtagh, R., Kniest, E. (2014). A comparison of multi- view 3D reconstruction of a rock wall using several cameras and a laser scanner. In Proceedings of ISPRS Technical Commission V Symposium, Riva del Garda, Italy, 23–25.

Torresan, C., Berton, A., Carotenuto, F., Di Gennaro, S. F., Gioli, B., Matese, A., ... , Wallace, L. (2017). Forestry applications of UAVs in Europe: A review. *International Journal of Remote Sensing, 38(8-10), 2427-2447.*

Wężyk, P., Szostak, M., Krzaklewski, W., Pająk, M., Pierzchalski, M., Szwed, P., Ratajczak, M. (2015). Landscape monitoring of post-industrial areas using LiDAR and GIS technology. *Geodesy and Cartography, 64(1), 125–137*. http://doi.org/10.1515/geocart-2015-0010

Zalesky, M., Zalesky, J., Kuklik, P., Hanek, P. (2008, May). Monitoring of a large slide and slope reclamation in a former Open-Pit Mine. In Proceedings of 13th FIG International Symposium on Deformation Measurements and Analysis and 4th IAG Symposium on Geodesy for Geotechnical and Structural Engineering.

Záleský, J., Čápova, K. (2017) Monitoring and assessment of remedial measures in closed open cast mine. In: Advancing culture of living with landslides, vol 3. *Springer International Publishing Switzerland. ISBN 978-3-319-53486-2*.

Zhou, Hailing, Kong, Hui, Wei, Lei et al. (2015) Efficient Road Detection and Tracking for Unmanned Aerial Vehicle. *IEEE TRANSACTIONS ON INTELLIGENT TRANSPORTATION SYSTEMS Volume: 16 Issue: 1 Pages: 297-309*.